



RESEARCH ARTICLE

10.1002/2016RS006089

Key Points:

- A phase calibration method that may be executed within an autonomous system is presented
- Backscatter with a known location is used to estimate the phase bias
- The calibrated elevation angle errors are reduced from several degrees to 1 degree or less

Correspondence to:

A. G. Burrell,
ab763@le.ac.uk

Citation:

Burrell, A. G., T. K. Yeoman, S. E. Milan, and M. Lester (2016), Phase calibration of interferometer arrays at high-frequency radars, *Radio Sci.*, 51, 1445–1456, doi:10.1002/2016RS006089.

Received 23 MAY 2016

Accepted 16 AUG 2016

Accepted article online 22 AUG 2016

Published online 8 SEP 2016

© 2016. The Authors.

This is an open access article under the terms of the Creative Commons Attribution License, which permits use, distribution and reproduction in any medium, provided the original work is properly cited.

Phase calibration of interferometer arrays at high-frequency radars

Angeline G. Burrell¹, Timothy K. Yeoman¹, Stephen E. Milan¹, and Mark Lester¹

¹Department of Physics and Astronomy, University of Leicester, Leicester, UK

Abstract Elevation angles of backscattered signals are calculated at the Super Dual Auroral Radar Network (SuperDARN) high-frequency radars using interferometric techniques. These elevation angles make it possible to estimate the geographic location of the scattering point, an essential piece of information for many ionospheric studies. One of the most difficult parameters to measure is the effective time delay caused by the difference in the electrical path length that connects the main array and the interferometer arrays to the correlator (δt_c). This time delay causes a bias in the measured difference in the signal phase, also known as a phase bias. Phase calibration is difficult due to unknown physical attributes of the hardware and the remote location of many radars. This leads to the possibility of sudden external changes, slow temporal drift, and a dependence on transmission frequency. However, it is possible to estimate δt_c using the radar observations themselves. This article presents a method for estimating δt_c using backscatter with a known location, such as backscatter from artificially generated irregularities, meteor echoes, or distinct groundscatter, which incorporates the uncertainty in the observations and may be used autonomously. Applying the estimated δt_c is shown to improve elevation angle uncertainties at one of the SuperDARN radars from their current potential tens of degrees to less than a degree.

1. Introduction

Coherent-scatter high-frequency (HF) radars work by sending a series of radio pulses out toward a scattering region and measuring the time it takes for the backscattered signal to return, the difference in phase between the transmitted and received signal, and the strength of the received signal. The transmitted radio waves will be refracted by the ionosphere, making it possible for signals to travel horizontally in the ionosphere or even return back to the ground. Appropriate scattering targets include ionospheric irregularities and rough surfaces on the ground. Ionospheric backscatter can be observed when ionospheric irregularities are aligned with the magnetic field at the point where the radio signal is perpendicular to the magnetic field line. Groundscatter can be observed when the radio signal is refracted down to the ground. Both ionospheric backscatter and groundscatter are observed by the Super Dual Auroral Radar Network (SuperDARN) [Greenwald *et al.*, 1995; Chisham *et al.*, 2007], which is made up of coherent-scatter HF radars that were deployed to observe the middle- and high-latitude ionosphere over the northern and southern poles. Many of the studies performed using the SuperDARN radars require knowledge of the exact location (latitude, longitude, and altitude) of the scattering location of the backscattered signal. This information can be obtained by combining the elevation angle of arrival with the azimuthal angle (or beam direction), the time of flight, and the location of the radar.

The time of flight for a signal to travel from and return to a SuperDARN radar is interpreted as a distance. The HF radar emits a multipulse signal at a frequency between 8 and 20 MHz along a narrow, steerable beam that lies at a specified azimuthal angle from the radar boresight. In standard operations, the returning signals are detected with a gate length of 300 μ s, translating to distance bins (or range gates) of 45 km. Higher-resolution modes are also possible and currently used for special operational programs.

The vertical angle of arrival, or elevation angle (Δ), can be determined with the aid of an interferometer, a second, smaller antenna array that is displaced from the main radar array. The phase lag (Ψ) between the signals observed at the two arrays, determined from the cross-correlation function of the combined signals, can be used to calculate Δ [Farley *et al.*, 1981]. The two arrays are typically separated by a distance of 100 m (a distance longer than one wavelength at even the lowest frequency used by SuperDARN), which results in a 2π ambiguity in Ψ and aliasing in Δ .

Apart from aliasing, uncertainty in the measurement of Ψ will cause errors in Δ . These errors can be caused by multipath propagation, self-clutter from the multipulse signaling method [Reimer and Hussey, 2015], uncertainty in the azimuth angle caused by the possibility of signals returning from both in front of and behind the main radar array [Milan et al., 1997a], and phase bias (δt_c), which results from a difference in the electrical paths that connect the main and interferometer arrays to the radar correlator [Baker and Greenwald, 1988]. Most of these sources of error are either corrected in the standard SuperDARN data analysis or can be corrected as a secondary processing step [Burrell et al., 2015]. Uncertainty in δt_c , however, is currently an issue at all radars with an interferometer. For example, at a HF radar setup as a standard SuperDARN radar (with a 100 m baseline between the main and interferometer arrays) an uncertainty in δt_c of 10 ns can cause, at the upper limit, elevation angle errors on the order of tens of degrees.

Currently, most SuperDARN radars use a frequency-independent measurement of δt_c , known as the hardware δt_c , which was determined by measuring the length of the cables that connect the main and interferometer arrays to the correlator and finding their difference. Unfortunately, the length and documented characteristics of the cables do not accurately describe the delay that the signal experiences under operational conditions and are known to have frequency-dependent electrical paths. It should also be noted that the physical properties of the radar hardware may change over time or be damaged, causing a change in δt_c that would not be known to operators who have radars at remote locations.

Past work has shown that it is possible to estimate δt_c for individual radars by using backscatter coming from a known location. This basic concepts holds true for any type of radar with an interferometer. For example, Gao and Mathews [2014] showed how coherent backscatter returning from satellites could be used to calibrate the phase and antenna patterns of the Jicamarca Radio Observatory (JRO) 50 MHz radar system.

The first published phase calibration of the SuperDARN radars used the altitude distribution of 7 years of meteor backscatter to estimate a frequency-independent offset at the Saskatoon and Prince George radars [Chisham and Freeman, 2013]. Unfortunately, to be operationally useful, methods to estimate δt_c must account for frequency and temporal variations.

More recently, Ponomarenko et al. [2015] presented a method of estimating δt_c using groundscatter observations. This method uses regions of backscatter that extend to far range gates and have roughly the same virtual height, such as groundscatter with virtual heights of 200–300 km. Because elevation angle aliasing will occur at the more distant range gates, δt_c may be arrived at incrementally, with the user adjusting δt_c manually to obtain elevation angles that show aliasing at the farthest range gates. The corrected elevation angles for the groundscatter will then produce virtual heights that are constant with increasing range gate. This alias-correcting method of δt_c estimation has several advantages: it requires a small amount of data, may be performed daily, and may be applied to all frequency bands that observe suitable backscatter populations. However, not all frequency bands detect suitable backscatter at the range gates where aliasing is expected, and there is a subjective element involved in the phase calibration.

This paper presents a method of estimating δt_c for HF radars that can be applied routinely or retrospectively to data sets that fulfill certain requirements. The estimation method presented here reduces the subjectivity involved in phase calibration by setting a mathematical criteria for an acceptable fit and may be automated when appropriate data can be selected automatically. Section 2 discusses the process of estimating δt_c , while section 3 looks at two different types of data that can be used to produce a reliable estimate. The estimation method is then validated in section 4. Finally, the conclusions are presented in section 5.

2. The δt_c Estimation

The SuperDARN elevation angles are calculated as shown in equation (1).

$$\Delta = \arcsin \sqrt{\cos^2 \alpha - \left(\frac{\Psi}{k d_{cor}} \right)^2} + \Delta_{cor}. \quad (1)$$

In this equation α is the azimuthal angle of the beam off the radar boresight at zero elevation, k is the wave number of the incoming signal, d_{cor} is the horizontal distance between the midpoints of the main and interferometer arrays, Δ_{cor} is the difference in elevation caused by the altitude difference between the main and interferometer arrays (which also depends on the azimuthal angle of the beam), and Ψ is the phase lag between signals received at the main and interferometer arrays. Ψ is specified by equation (2), in which L is

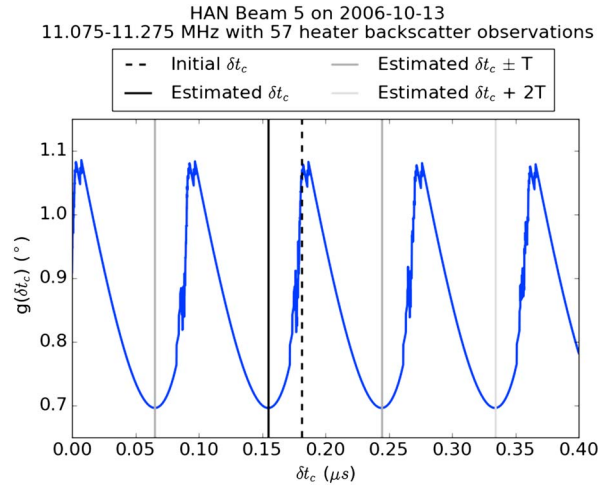


Figure 1. Minimization of $g(\delta t_c)$ using backscatter observed from Hankasalmi at a known latitude as a function of δt_c . The initial and estimated δt_c are shown as dashed and solid black lines, respectively. The grey lines show where δt_c estimates would lie with $LfT = \pm 1$ or ± 2 determining the period, T .

which can be calculated using the location of the radar, the beam direction, the time of flight (or range gate), and Δ can be used to obtain a known Δ if l has been determined using a different instrument. This known location will be referred to as l_0 , and the backscattered signals that return from the scattering target lying at this location will be referred to as the selected data set. Not restricting l to a particular geographic coordinate (such as only altitude or latitude) maximizes the situations where this phase calibration method can be used.

If there are sufficient observations in the selected data set for a given frequency band, δt_c can be estimated by optimizing the distribution of l about l_0 . This function describes the typical deviation of backscatter about a desired location, using the mean and standard deviation of the backscatter distribution:

$$g(\delta t_c) = \sqrt{(\bar{l} - l_0)^2 + \sigma_l^2}, \quad (3)$$

where \bar{l} is the mean and σ_l is the standard deviation of the scattering target locations calculated for the selected backscatter. By considering the first and second moments of the location distribution, bimodal distributions that populate each side of the desired location are eliminated. Testing determined that $g(\delta t_c)$ requires a minimum of 50 observations to prevent the formation of spurious peaks with the potential to interfere with the function minimization. The frequency bands used to limit the selected data set should reflect the range of frequencies scanned in the different operational modes. The initial guess for the δt_c estimate is the hardware δt_c , since it is the current best estimate.

The minimization process is performed using a simplex method [Nelder and Mead, 1965], which searches for local minima in $g(\delta t_c)$ without the need for bounds, derivatives, or a global minimum. Additional tests to improve the robustness have also been applied, ensuring that the local minimum selected is one of the grand minima closest to the initial δt_c . This is done by identifying the grand minima on either side of the initial δt_c , and selecting the grand minima closest to the initial guess. This process is illustrated in Figure 1. To ensure that both of the identified minima optimize $g(\delta t_c)$ equally well, $g(\delta t_c)$ at these minima are required to differ by no more than a tolerance value. In the case that one minimum is more significant than the other, the deeper minimum is chosen. In practice, however, the cyclical nature of $g(\delta t_c)$ means that this does not happen.

The initial choice for δt_c is important for examining temporal variations but does not ultimately affect the calculation of the elevation angle. The unspecified ambiguity, n , in Ψ causes an ambiguity in δt_c that manifests as a periodic $g(\delta t_c)$. Since the period between the grand minima (T) introduces an integer ambiguity into Ψ , it will be removed along with n when Δ is calculated. The integer nature of the additional ambiguity introduced by δt_c can be confirmed by using equation (2) to calculate T . Replacing δt_c with $\delta t_c + T$,

$$\Psi = L [\Psi_0 + 2\pi f \delta t_c] + 2\pi [n + LfT]. \quad (4)$$

the sign determined by the backscatter origin field of view, Ψ_0 is the measured phase lag between the signals received at the main and interferometer arrays, f is the transmission frequency in megahertz, and n is the integer ambiguity introduced by the separation of the main and interferometer arrays [Milan et al., 1997b].

$$\Psi = L [\Psi_0 + 2\pi f \delta t_c] + 2n\pi. \quad (2)$$

When Ψ_0 is measured and L is known or determined using the method described by Burrell et al. [2015], δt_c (in μs) can be determined for backscatter returning with a known Δ by combining equations (1) and (2).

While there are no independent observations of Δ , it is possible to calculate the elevation angle using observations of quantities that depend on Δ . The geographic location of a scattering target (l),

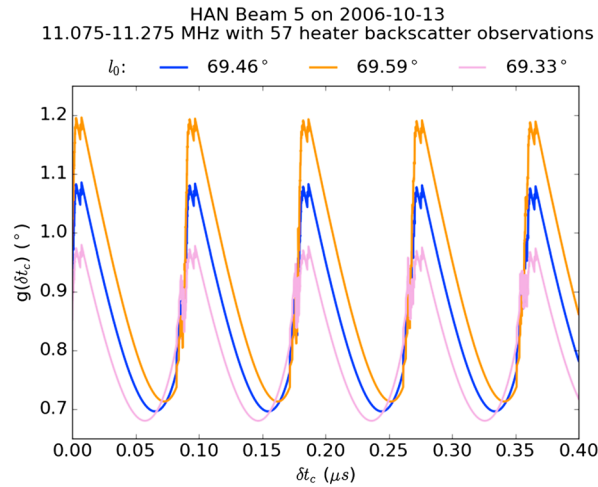


Figure 2. $g(\delta t_c)$ using backscatter observed from Hankasalmi at a known latitude as a function of δt_c for three different l_0 . The blue line uses the reference latitude, while the orange and plum lines alter this latitude by $\pm 0.13^\circ$.

The accuracy of l_0 is also important. When the wrong l_0 is used, $g(\delta t_c)$ must compromise minimizing the spread of the location distribution and centering the distribution about l_0 . Figure 2 shows how $g(\delta t_c)$ changes with a difference in l_0 of 0.13° latitude. This difference in latitude causes δt_c to shift by about 7 ns, which would result in an error in Δ on the order of a degree for the selected frequency band.

The integer ambiguity present in the δt_c estimates makes it possible to establish the maximum range of error possible in δt_c at different frequencies. Figure 3 shows the frequency-independent hardware value of δt_c at Hankasalmi, along with the nearest (lower) equivalent δt_c as a function of frequency. The different operational frequency bands for the Hankasalmi radar are shown as grey boxes within the two limits, highlighting the range of possible correction at each frequency band.

Although precautions have been taken to avoid situations where $g(\delta t_c)$ cannot be minimized, there is always the possibility that the solution will not converge. In cases where δt_c cannot be determined to an accuracy of 0.1 ns within 2000 iterations, an empirically determined threshold, no estimated δt_c is returned. Such instances typically indicate that the selected backscatter originate from two or more distinct locations.

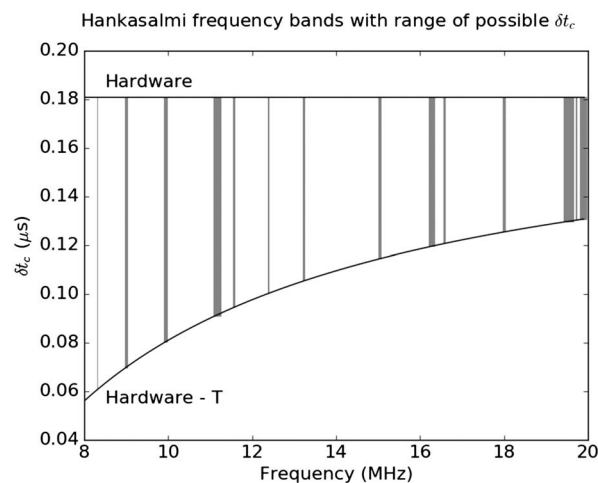


Figure 3. Range of δt_c below the δt_c specified by the radar hardware file as a function of frequency. The grey bars show the frequency bands in which Hankasalmi is allowed to operate.

Thus, when LfT is an integer, no error is introduced by selecting any one of the grand minima of $g(\delta t_c)$. Figure 1 shows that this is the case. The grey lines in the figure show what the value of δt_c would be with $LfT = \pm 1$ or ± 2 . The grey lines fall at the minima surrounding the minima containing the estimated δt_c , confirming that any grand minima provides a δt_c estimate that will remove the phase bias in Δ .

The validity of the δt_c estimation relies first and foremost on accurately selecting the backscatter. Backscatter from two locations will create a bimodal distribution when the correct δt_c is used to compute the location. However, since $g(\delta t_c)$ is designed to reject bimodal distributions the minimization will not arrive at the correct δt_c .

3. Selecting Data

Although any coordinate that can be calculated from Δ and from an independent measurement may be used, some location coordinates are easier to obtain than others. The previous section used latitude as an example. Another possible location coordinate is altitude. Whichever coordinate is used, the backscatter range accuracy will influence the quality of the phase calibration. Past studies into the range accuracy at the CUTLASS (Cooperative UK Twin Auroral Sounding System) radars have found uncertainties in slant distance between 16 km and 165 km, depending on the propagation path, frequency, range gate size, and geolocation

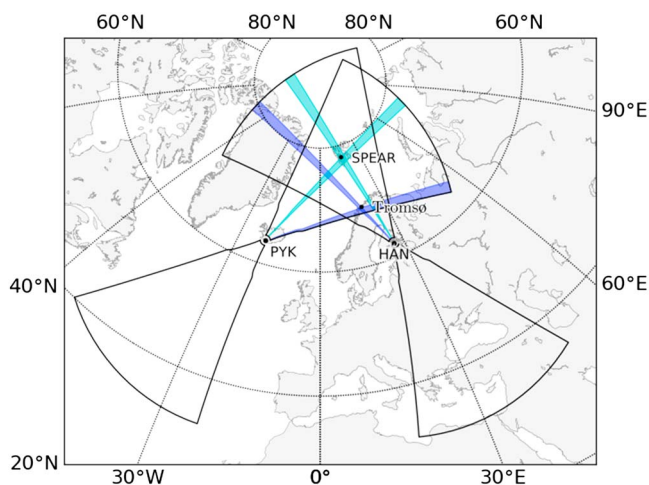


Figure 4. Map of the CUTLASS radar fields of view with the SPEAR and Tromsø heater locations. The blue and cyan shaded areas show the radar beams that detect the strongest signals from irregularities generated by the Tromsø and SPEAR heaters, respectively.

model used [Yeoman *et al.*, 2001, 2008b]. The uncertainty in slant range is managed by choosing an appropriate number of observations to use in the optimization. Because this uncertainty is not systematic, it only influences the range of values σ_r may take and does not affect the δt_c estimate.

3.1. Artificially Created Irregularities

Ionospheric heaters, HF transmitters that pump energy into the *F* region, cause plasma irregularities with scale sizes appropriate for observation by SuperDARN. The European Incoherent Scatter Scientific Association (EISCAT) operates several heaters. The EISCAT heaters, which are (or were) located alongside the incoherent scatter radars, include one at Tromsø [Stubbe *et al.*, 1982] and another at Svalbard [Robinson *et al.*, 2006]. The heater at Svalbard, also known as the Space Plasma Exploration by Active Radar (SPEAR), was operational for a limited period of time (2004–2010). When the incoherent scatter radars (ISRs) are used to provide I_0 for the phase calibration, the uncertainty in I_0 is typically much smaller than the range resolution of the SuperDARN backscatter and so may be neglected [Shergill *et al.*, 2010].

Irregularities created by the Tromsø and SPEAR heaters are visible from the SuperDARN radars at Hankasalmi and Bykkvibær, as illustrated in Figure 4. The Tromsø heater creates irregularities that are visible along a $\frac{1}{2}$ -hop propagation path (the signal encountered the irregularity without ever scattering from the ground) from Hankasalmi and along a $1\frac{1}{2}$ -hop propagation path (the signal scattered forward from the ground before encountering an irregularity in the ionosphere and scattering backward) from Bykkvibær, while SPEAR irregularities are observed along $1\frac{1}{2}$ -hop propagation paths from both of these radars. A more detailed explanation of the propagation path nomenclature can be found in Milan *et al.* [1997b], while ray tracing of the $1\frac{1}{2}$ -hop propagation path between a HF radar and an ionospheric heater can be found in Yeoman *et al.* [2008b].

F region irregularities can be formed by an ionospheric heater or pump within the upper hybrid plane, a narrow altitude band below the ordinary (*O*-mode) reflection height, where the radio waves are converted to electrostatic modes that cause small-scale density striations [e.g., Robinson, 2002]. Shergill *et al.* [2010] statistically examined the spatial distribution of irregularities created by the Tromsø heater and observed by the CUTLASS radars, showing that the irregularities tend to coalesce along magnetic field lines. This allows the latitude of the heater irregularity to be found by measuring the irregularity altitude with an ISR and tracing up the magnetic field line that intersects the heater.

One might wonder why the examples in section 2 used latitude as the location coordinate instead of height, since height is the location coordinate measured for the irregularities. The virtual height, h' , of backscatter can be specified by considering the oblique triangle, illustrated in Figure 5, which reaches from the center of the Earth (origin of the coordinate system), to the radar (the magenta point labeled r), to the ionospheric reflection point (light blue point labeled i'). In this figure, R_r is the terrestrial radius at the radar location and d is the distance to the ionospheric refraction point, measured as the time of flight and recorded in range gates for direct ($\frac{1}{2}$ -hop) ionospheric propagation paths. The equation below finds h' by solving for R_i , the distance

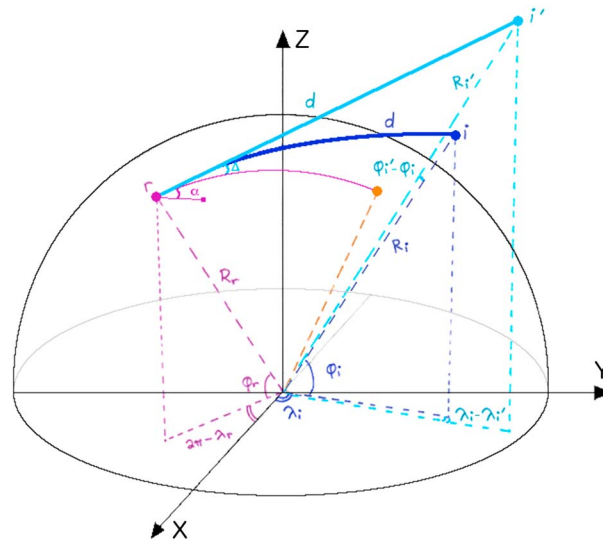


Figure 5. Sketch of a $\frac{1}{2}$ -hop propagation path that is refracted by the ionosphere before reflecting from the field-aligned irregularity (dark blue point, i). If the amount of refraction is not known, the latitude, longitude, and radial distance of the straight-line path (light blue point, i') can be found ($\phi_{i'}$, $\lambda_{i'}$, and $R_{i'}$, respectively) when the radar location (magenta point, r), boresight location (small magenta dot), azimuthal beam angle (α), elevation angle (Δ), and slant distance (d) are known. The orange point marks the ionospheric heater.

from the center of the Earth to i' , which is equal to h' plus R_r .

$$h' = \sqrt{d^2 + R_r^2 + 2dR_r \sin \Delta} - R_r. \quad (5)$$

The virtual height typically overestimates the true height (h), since the transmitted signal will be refracted by the ionosphere before encountering field-aligned irregularities in the E or F region ionosphere [Chisham *et al.*, 2008].

The latitude of the backscatter reflection point can be calculated using Δ , d , R_r , α , the location of the radar in geographic latitude (ϕ_r), and longitude (λ_r). These can be used to identify the straight-line projection of the irregularity location ($\phi_{i'}$, $\lambda_{i'}$), as illustrated in Figure 5. The refraction of the transmitted signal causes differences between the real irregularity location (i) and i' , overestimating $R_{i'}$ and underestimating $\phi_{i'}$ and $\lambda_{i'}$. At Hankasalmi, where the central beams are aligned with the geographic meridian, the difference between ϕ_i and $\phi_{i'}$ will increase with longer ranges and greater hops. For example, ray tracing shows that at 11.175 MHz the latitude at Tromsø along a $\frac{1}{2}$ -hop path is underestimated by about 0.1° while the latitude at SPEAR along a $1\frac{1}{2}$ -hop path is underestimated by about 2.5° . Figure 2 illustrated the influence a measured uncertainty on the order of a tenth of a degree would have on the phase calibration. Thus, estimates at Hankasalmi are preferentially made using irregularities created by the Tromsø heater.

An example of δt_c estimation made using $\frac{1}{2}$ -hop backscatter from a field-aligned irregularity induced by the Tromsø heater is shown in Figure 6. These are the same data that were used as an example in section 2 and have been previously presented by Blagoveshchenskaya *et al.* [2009]. Figure 6 (left) shows the available and selected backscatter. The boxes in this panel mark the times when there was O -mode heating, which leads to the creation of ionospheric irregularities that disperse when the source of heating is removed. When selecting the heater irregularity backscatter, it is important to choose the frequency band that measures the highest power during the O -mode heating times. This figure uses observations from beam 5, frequencies between 11.075 and 11.275 MHz, and special operational program designed to observe ionospheric heating, which uses standard 45 km range gates and fine-tuned transmission frequencies. Backscatter returning from the heater irregularities were selected by choosing times with powers of at least 10 dB at range gates 10–25. This returns 57 backscatter points, which are marked by black dots. Figure 6 (right) contains histograms showing the latitude distributions of the selected ionospheric backscatter with the hardware and estimated δt_c .

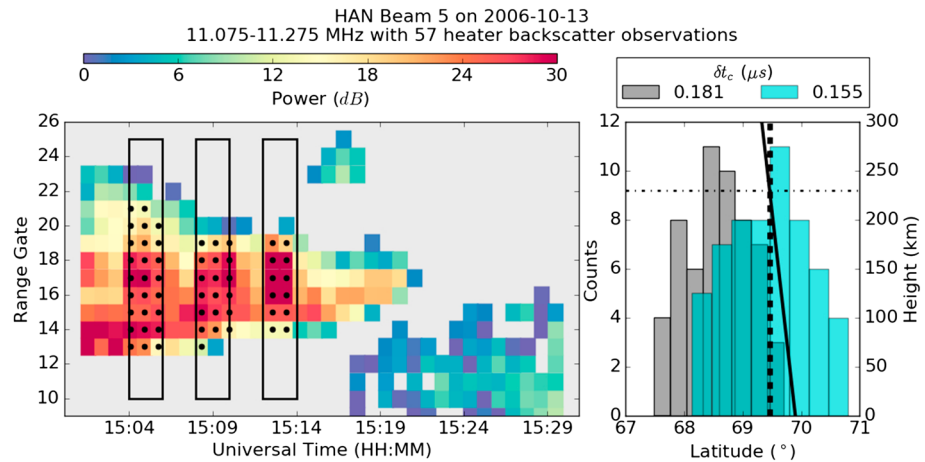


Figure 6. Heater irregularity selection and location. (left) The Hankasalmi backscatter for beam 5 as a function of time, range gate, and power with dots showing the selected data and boxes denoting times and the heater was operational. (right) The latitude distributions for the selected backscatter calculated using the hardware (grey) and estimated (cyan) δt_c . This panel also shows the Tromsø magnetic field line (solid), the measured height of the artificial irregularity (dash-dotted) with uncertainty (dotted), and the corresponding latitude (dashed).

Figure 6 (right) also shows the magnetic field line over Tromsø, illustrating the process used to convert from irregularity altitude of 230 km to latitude.

3.2. Meteor Scatter

Ionospheric backscatter from meteor echoes provide a data set where altitude can be used to estimate δt_c . Figure 5 illustrates the effect that ionospheric refraction can have on the path a HF signal travels before encountering an irregularity. However, when backscatter returns from altitudes low enough that the ionospheric density was unable to cause refraction and a distance close enough to the radar that the curvature of the Earth can be considered negligible, the real and virtual heights are equal. When these conditions are met, it is appropriate to use h to estimate δt_c .

Meteor echoes provide backscatter that meet the conditions for equality between h and h' . Two populations of meteor echoes are observed by radars: overdense and underdense. Overdense echoes occur in regions where the density of the plasma created by the meteor ablation is large enough to completely reflect the transmitted radio wave, while underdense echoes are detected in regions where the plasma density is low enough that radio waves are scattered by individual free electrons along the meteor trail. The ionospheric altitude band that allows this type of meteor echo (the D region) is narrow and located well below the primary ionospheric layers.

The use of h and meteor echoes in δt_c estimation is tested in Figure 7 by creating a modeled set of meteor echoes. A modeled data set is used to allow testing of the reliability of the estimation method using a second data set, as well as testing of the robustness required in the selected backscatter to produce a reliable δt_c estimate. Figure 7 (top) shows the altitude distribution of the modeled backscatter, which consists of 150 points selected randomly from a Gaussian distribution centered at 90 km with a standard deviation of 5 km. The beams and frequencies of the modeled backscatter were randomly set within the realistic limits, 0–15 for the beams and 8.305–8.335 MHz for the transmission frequency (using the lowest frequency band at Hankasalmi). The first range gate was used, giving $d = 180$ km. A single range gate was used because the mean height at which meteor echoes are observed changes with range gate [Chisham and Freeman, 2013]. The initial δt_c was set to the hardware value at Hankasalmi, while the true δt_c was declared to be 0.140 μs .

Figure 7 (bottom) shows the Δ distributions. The true Δ are shown in grey and the Δ calculated with the hardware δt_c in cyan. Finally, the Δ calculated with the δt_c estimated using the modeled meteor echoes is shown in yellow. There is a 0.8 ns difference between the true and estimated δt_c , which results in elevation angle errors on the order of 0.1°.

As stated in section 2, the selection of meteor echoes is very important for estimating δt_c . E region backscatter is also observed at the same range gates as meteor echoes. If sufficient E region backscatter is included

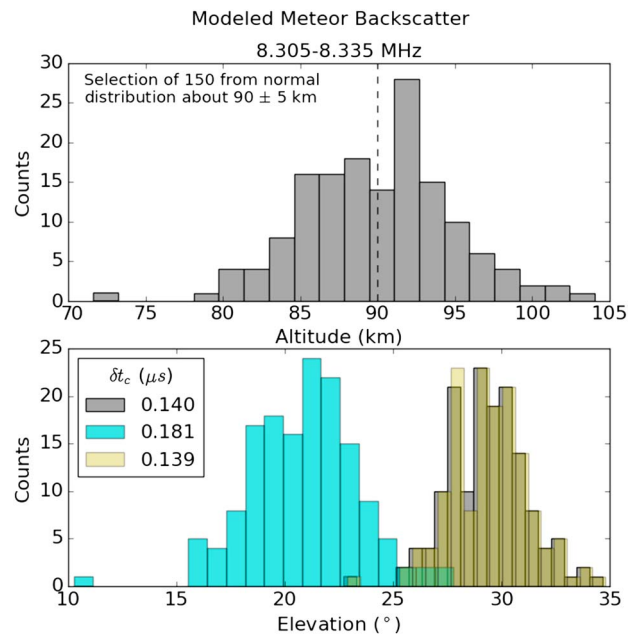


Figure 7. Modeled meteor backscatter for the lowest frequency band at Hankasalmi. The 150 *D* region echoes were randomly selected from a Gaussian distribution centered at 90 km. (top) The altitude distribution of this selection is shown; (bottom) the elevation distribution for three different values of δt_c . Grey shows the true δt_c , cyan the hardware value, and yellow shows the estimated value.

in the estimation process, the resulting δt_c estimation will be wrong. Figure 8 demonstrates the effects of different levels of *E* region contamination on the δt_c estimation. *E* region backscatter was generated using a random selection from a Gaussian centered at 115 km with a standard deviation of 10 km. The different panels show the different levels of contamination. It can be seen that the δt_c estimations with contamination levels over 15% are not reliable, showing deviations from the true δt_c near 10 ns (or elevation angle deviations on the order of a degree). Therefore, it is essential to remove nearly all *E* region backscatter when using meteor echoes to estimate δt_c . While the backscatter available from historical data sets proved to have too high of a contamination level to use, it is possible to design an operational program to select meteor echoes [Tsutsumi *et al.*, 2009]. Using observations from such a program will make it possible to estimate δt_c at any HF radar on a regular basis.

4. Validation

This section tests the validity of the δt_c estimation method in two ways. First, this δt_c estimation is tested against a heating period at SPEAR. Second, the same δt_c estimate is tested using groundscatter, following the method developed by Ponomarenko *et al.* [2015]. The estimate being tested was made at Hankasalmi for frequencies between 11.075 and 11.275 MHz on 13 October 2006, using observations from an irregularity generated by the ionospheric heater at Tromsø. Blagoveshchenskaya *et al.* [2009] presented data for this heating period from three of these frequency bands, though a fourth frequency band (which is used in this section and in the examples of the δt_c estimation process in section 2) provided the clearest observations of the artificial irregularities.

4.1. Tromsø-SPEAR Validation

On 12 October 2006, SPEAR was operational, creating ionospheric irregularities that were detected through a $\frac{1}{2}$ -hop path by Hankasalmi. Yeoman *et al.* [2008a] used this data to study ULF wave structures. The following day, the Tromsø heater was operational and the Hankasalmi radar observed the artificially induced irregularities most strongly in the same frequency band along a $\frac{1}{2}$ -hop path, presented in sections 2 and 3.2.

Figure 9 shows the SPEAR heater observations taken by Hankasalmi along beam 9 on 12 October 2006 for frequencies between 11.075 and 11.275 MHz. The backscatter points were selected by limiting range gates and selecting powers greater than 10 dB. Figure 9 (first row) shows the Doppler velocities for the same period

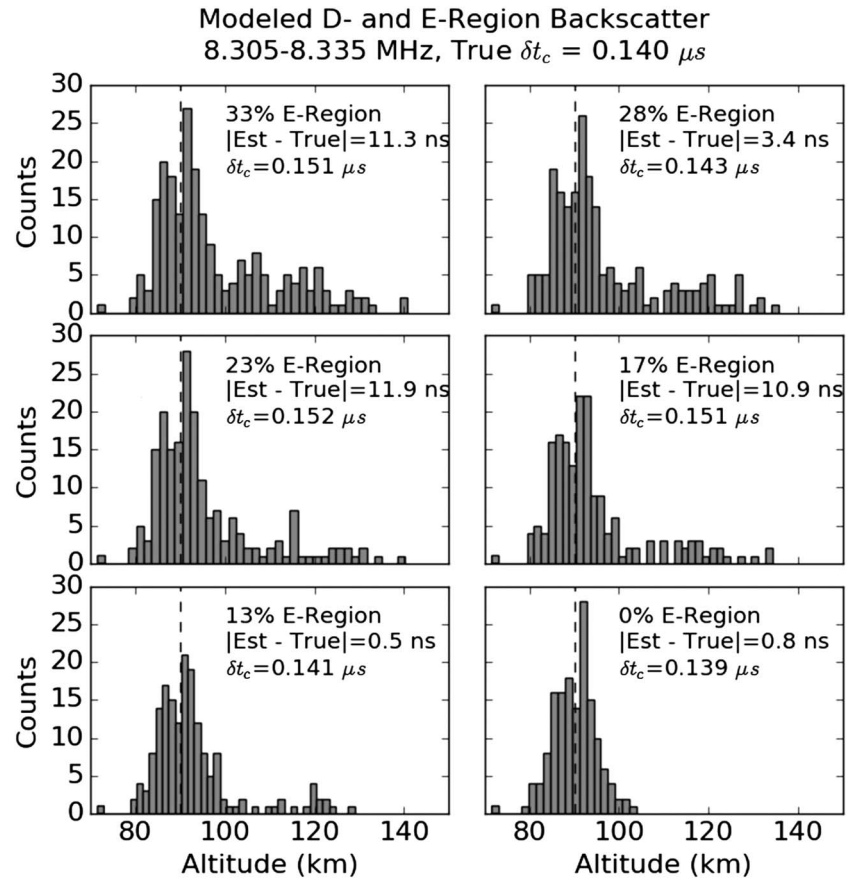


Figure 8. Modeled meteor backscatter for the lowest frequency band at Hankasalmi with different levels of *E* region contamination. Between 22 and 75 *E* region observations were added to the 150 *D* region echoes. Each panel shows the altitude distribution of the contaminated data sets, with the bottom right panel showing the uncontaminated data set. The estimated δt_c and their deviation from the value are recorded in the upper right corner of each panel.

of time as Figure 4 from *Yeoman et al. [2008a]* (though *Yeoman et al. [2008a]* used Hankasalmi observations taken using frequencies between 12.370 and 12.415 MHz).

Figure 9 (fourth row) shows the latitude distribution of the heater backscatter using the hardware δt_c (grey) and the δt_c estimated at Tromsø along beam 5 (cyan). The uncorrected heater backscatter is seen to have two populations, with the majority of the backscatter lying to the north of the heater. The presence of two distinct populations suggest that when the hardware δt_c is used to calculate the elevation angle, inappropriate aliasing (a feature used by *Ponomarenko et al. [2015]* in their estimation technique) is occurring. When the elevation angle is corrected using the estimated δt_c , however, a single population with a mean latitude at the expected irregularity latitude (found by tracing up the field line intersecting the ionospheric heater to an altitude of 215 km) is formed.

Figure 9 (second and third rows) examines the latitude distribution for the heater backscatter in more detail. Figure 9 (second row) shows the latitudes calculated using the hardware δt_c , and Figure 9 (third row) uses the estimated δt_c . The latitude variation in Figure 9 (third row) follows the temporal changes in range gate seen in the irregularity in Figure 9 (first row), suggesting these latitude variations reflect real location changes in the irregularity. The good geolocation of this irregularity is reassuring, since a systematic underestimation of *l* introduced through using a straight-line approximation for the $\frac{1}{2}$ -hop backscatter path in the δt_c estimate would not lead to such good agreement along a $1\frac{1}{2}$ -hop propagation path. This implies that the error introduced by neglecting ionospheric refraction is typically smaller than the uncertainty in range.

4.2. Groundscatter Validation

Figure 10 uses groundscatter detected in the front field of view at Hankasalmi on 12 October 2006 using the 11.075–11.275 MHz frequency band in beam 7 to evaluate the δt_c estimation performed on 13 October

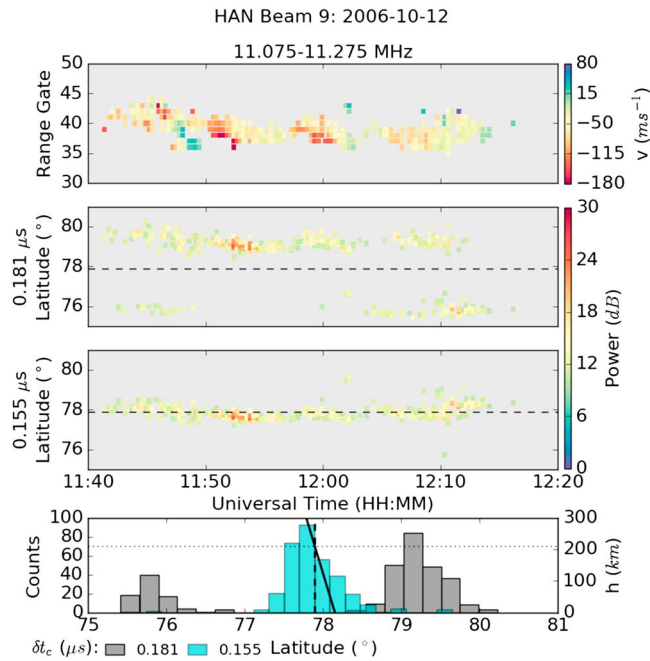


Figure 9. SPEAR heating event on 12 October 2006 used to validate the δt_c estimate made at Tromsø on 13 October 2006. The first row shows heater backscatter as a function of time, range gate, and Doppler velocity. The heater backscatter as functions of time, latitude, and power with latitude calculated using the hardware δt_c (second row) and the estimated δt_c (third row). The fourth row shows the latitude distribution of the heater backscatter for the hardware (grey) and estimated (cyan) δt_c . The dashed black lines (second to fourth rows) show the latitude corresponding to an altitude of 215 km (black dotted line) along the SPEAR magnetic field line (solid black line).

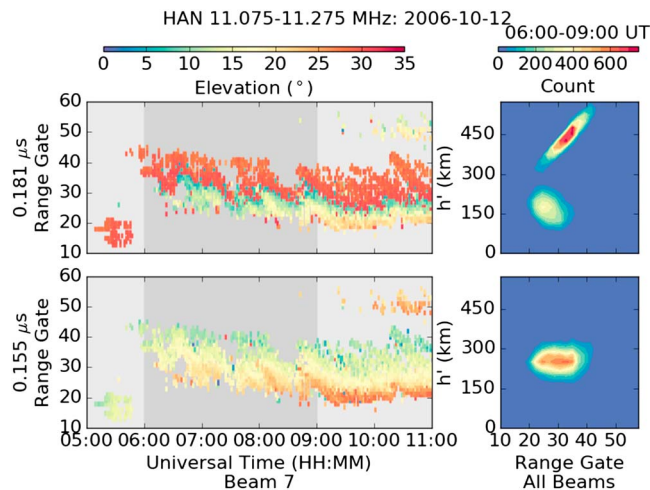


Figure 10. Groundscatter observed from Hankasalmi on 12 October 2006 used to validate the δt_c estimate made at Tromsø on 13 October 2006. The left column shows groundscatter as a function of time, range gate, and elevation angle for the front field of view along beam 7. The right column shows two-dimensional histograms of the virtual height for the groundscatter observed returning from the front field of view along all beams between 06:00 and 09:00 UT (highlighted by the dark grey boxes (left column)). (top row) The rows show data calculated using the hardware (top) and estimated (bottom) δt_c .

2006. Figure 10 (left column) shows the groundscatter as function of universal time (UT), range gate, and Δ . Figure 10 (right column) shows two-dimensional histograms of h' for the groundscatter observed returning between 06:00 and 09:00 UT, highlighted by the dark grey box in Figure 10 (left column), but for all beams. Figure 10 (top row) shows these data calculated using the hardware δt_c , while the Figure 10 (bottom row) uses the estimated δt_c .

The main groundscatter structure, starting just before 06:00 UT at range gate 45 and widening to cover range gates 20–45 by 11:00 UT, shows consistent aliasing at range gates 30–35. This causes two h' populations to form in the histogram, neither of which has a constant value with increasing range gate. When the δt_c estimated using Tromsø irregularities is used, however, the majority of groundscatter at all range gates is seen to lie near 250 km. The groundscatter structures in Figure 10 (left column) now show the expected decrease in elevation angle with increasing range gate, with some aliasing present in the main groundscatter structure. This aliasing occurs for a few scattered points, primarily at the more distant range gates. The variation in range gate for the aliased points reflects the altitude variations in the groundscatter structure, created by atmospheric gravity waves (note the elevation angle striations traveling toward the radar) disturbing the ionosphere at this time.

5. Conclusions

Problems measuring δt_c , a hardware bias that causes an offset in the phase lag, has introduced uncertainty on the order of several degrees into SuperDARN elevation angles. However, it is possible to provide accurate estimates of δt_c using backscatter at a known location. Although the concept is not new, the δt_c estimation method presented in this article allows phase calibration to be performed for a variety of conditions, and has the capability to be automated.

$\frac{1}{2}$ -hop ionospheric backscatter returning from heater-generated irregularities has been used to estimate δt_c at Hankasalmi. The error of such estimates depends first and foremost on choosing the right backscatter observations to use in the estimation process. Uncertainty is also introduced through the error in the independent measurement of the backscatter location and the method used to calculate the location of the backscatter target. For artificial irregularities with independent location measurements provided by incoherent scatter radars, the error introduced by using a straight-line approximation contributes most to the uncertainty in δt_c . However, validation of $\frac{1}{2}$ -hop backscatter estimates show that the δt_c estimates are accurate to within 1 ns.

Existing heating experiments at the SPEAR and Tromsø ionospheric heaters can also be used to provide δt_c estimates for Þykkvibær, though care must be taken to validate these estimates as observations would be made along $1\frac{1}{2}$ -hop propagation paths. Tromsø will also lie within in the field of view of a SuperDARN radar currently being deployed in the south of France, further motivating regular heating experiments to track δt_c at these European radars. American ionospheric heating experiments observed at Kodiak [e.g., Hughes *et al.*, 2003] and rocket experiments would also be appropriate.

The method presented in this paper may be used for any population of backscatter with a known location coordinate, not just ionospheric backscatter from artificial irregularities. Groundscatter returning from a fixed location, such as a narrow coastline or mountain peak, would be appropriate. A transponder would also provide a clear signal from a known location. Ionospheric backscatter returning from underdense meteor ablation has been shown to work as well. The model populations of meteor echoes show that δt_c estimates made using data sets contaminated with less than 15% of backscatter from a different population differ from the truth δt_c by less than 1 ns. This suggests that meteor echoes are capable of providing δt_c estimates with a similar uncertainty as the heater irregularities.

Ionospheric backscatter from meteor echoes is commonly observed near the radar and are known to originate from a narrow range of heights in the D region ionosphere. Estimating δt_c from meteor scatter using historical data, however, was untenable at Hankasalmi since E region backscatter contamination proved to be a significant barrier when the elevation angle could not be included in the data selection criteria. In the future, however, programs designed to observe meteor backscatter (an operational program that saves data obtained at distances closer to the radar than the standard first range gate) can be used to provide δt_c estimates.

The wide range of data sets that can be used to estimate δt_c improves the range of frequencies that any particular radar will be able to accurately process. Historical data sets can be improved at select locations

using irregularities or groundscatter where the scattering location is known. Future radar operations can be improved by identifying or providing an appropriate scattering target. The efficiency of such efforts may be improved when a backscatter population at a known location can be automatically identified and supplied with a true location.

Acknowledgments

This study was supported by NERC grant NE/K011766/1. A python implementation of this estimation process is available as part of the DaViTpy python toolkit in the `davitpy/pydarn/radar/tdiff` directory. At the time of publication, this code can be found in the `develop` branch. The authors would like to thank Xueling Shi and Muhammad Rafiq of Virginia Tech for testing the code. The Virginia Tech SuperDARN database (`sftp://sd-data.ece.vt.edu`) is automatically accessed by the DaViTpy python toolkit. This toolkit contains up-to-date public access usernames and passwords that may be used to access the data without installing DaViTpy.

References

- Baker, K. B., and R. A. Greenwald (1988), The vertical angle of arrival of high-frequency signals propagating from Thule to Goose Bay, *J. Hopkins Apl. Tech. D*, *9*, 121–130.
- Blagoveshchenskaya, N. F., H. C. Carlson, V. A. Kornienko, T. D. Borisova, M. T. Rietveld, T. K. Yeoman, and A. Brekke (2009), Phenomena induced by powerful HF pumping towards magnetic zenith with a frequency near the F-region critical frequency and the third electron gyro harmonic frequency, *Ann. Geophys.*, *27*, 131–145.
- Burrell, A. G., S. E. Milan, G. W. Perry, and T. K. Yeoman (2015), Automatically determining the origin direction and propagation mode of high-frequency radar backscatter, *Radio Sci.*, *50*, 1225–1245, doi:10.1002/2015RS005808.
- Chisham, G., and M. P. Freeman (2013), A reassessment of SuperDARN meteor echoes from the upper mesosphere and lower thermosphere, *J. Atmos. Sol. Terr. Phys.*, *102*, 207–221, doi:10.1016/j.jastp.2013.05.018.
- Chisham, G., T. K. Yeoman, and G. J. Sofko (2008), Mapping ionospheric backscatter measured by the SuperDARN HF radars. Part 1: A new empirical virtual height model, *Ann. Geophys.*, *26*(4), 823–841, doi:10.5194/angeo-26-823-2008.
- Chisham, G., et al. (2007), A decade of the Super Dual Auroral Radar Network (SuperDARN): Scientific achievements, new techniques and future directions, *Surv. Geophys.*, *28*(1), 33–109, doi:10.1007/s10712-007-9017-8.
- Farley, D. T., H. M. Ierlik, and B. G. Fejer (1981), Radar interferometry: A new technique for studying plasma turbulence in the ionosphere, *J. Geophys. Res.*, *86*(A3), 1467–1472, doi:10.1029/JA086iA03p01467.
- Gao, B., and J. D. Mathews (2014), Phase and pattern calibration of the Jicamarca Radio Observatory radar using satellites, *Mon. Not. R. Astron. Soc.*, *446*(4), 3416–3426, doi:10.1093/mnras/stu2177.
- Greenwald, R. A., et al. (1995), DARN/SUPERDARN, *Space Sci. Rev.*, *71*(1–4), 761–796, doi:10.1007/BF00751350.
- Hughes, J. M., W. A. Bristow, R. T. Parris, and E. Lundell (2003), SuperDARN observations of ionospheric heater-induced upper hybrid waves, *Geophys. Res. Lett.*, *30*(24), 2276, doi:10.1029/2003GL018772.
- Milan, S. E., T. B. Jones, T. R. Robinson, E. C. Thomas, and T. K. Yeoman (1997a), Interferometric evidence for the observation of ground backscatter originating behind the CUTLASS coherent HF radars, *Ann. Geophys.*, *15*(1), 29–39, doi:10.1007/s00585-997-0029-y.
- Milan, S. E., T. K. Yeoman, M. Lester, E. C. Thomas, and T. B. Jones (1997b), Initial backscatter occurrence statistics from the CUTLASS HF radars, *Ann. Geophys.*, *15*(6), 703–718, doi:10.1007/s00585-997-0703-0.
- Nelder, J. A., and R. Mead (1965), A simplex method for function minimization, *Comput. J.*, *7*(4), 308–313.
- Ponomarenko, P., N. Nishitani, A. V. Oinats, T. Tsuya, and J.-P. S. Maurice (2015), Application of ground scatter returns for calibration of HF interferometry data, *Earth Planets Space*, *67*, 138, doi:10.1186/s40623-015-0310-3.
- Reimer, A. S., and G. C. Hussey (2015), Estimating self-clutter of the multiple-pulse technique, *Radio Sci.*, *50*, 698–711, doi:10.1002/2015RS005706.
- Robinson, T. R. (2002), Effects of multiple scatter on the propagation and absorption of electromagnetic waves in a field-aligned-striated cold magneto-plasma: Implications for ionospheric modification experiments, *Ann. Geophys.*, *20*, 41–55.
- Robinson, T. R., T. K. Yeoman, R. S. Dhillon, and M. Lester (2006), First observations of SPEAR-induced artificial backscatter from CUTLASS and the EISCAT Svalbard radars, *Ann. Geophys.*, *24*, 291–309, doi:10.5194/angeo-24-291-2006.
- Shergill, H., T. R. Robinson, R. S. Dhillon, M. Lester, S. E. Milan, and T. K. Yeoman (2010), A statistical study of the spatial distribution of Co-operative UK Twin Located Auroral Sounding System (CUTLASS) backscatter power during EISCAT heater beam-sweeping experiments, *J. Geophys. Res.*, *115*, A05307, doi:10.1029/2009JA014659.
- Stubbe, P., H. Kopka, H. Lauche, and M. T. Rietveld (1982), Ionospheric modification experiments in northern Scandinavia, *J. Atmos. Terr. Phys.*, *44*(12), 1025–1041.
- Tsutsumi, M., A. S. Yukimatu, D. A. Holdsworth, and M. Lester (2009), Advanced SuperDARN meteor wind observations based on raw time series analysis technique, *Radio Sci.*, *44*, RS2006, doi:10.1029/2008RS003994.
- Yeoman, T. K., D. M. Wright, A. J. Stocker, and T. B. Jones (2001), An evaluation of range accuracy in the Super Dual Auroral Radar Network over-the-horizon HF radar systems, *Radio Sci.*, *36*(4), 801–813, doi:10.1029/2000RS002558.
- Yeoman, T. K., L. J. Baddeley, R. S. Dhillon, T. R. Robinson, and D. M. Wright (2008a), Bistatic observations of large and small scale ULF waves in SPEAR-induced HF coherent backscatter, *Ann. Geophys.*, *26*, 2253–2263, doi:10.5194/angeo-26-2253-2008.
- Yeoman, T. K., G. Chisham, L. J. Baddeley, R. S. Dhillon, T. J. T. Karhunen, T. R. Robinson, A. Senior, and D. M. Wright (2008b), Mapping ionospheric backscatter measured by the SuperDARN HF radars—Part 2: Assessing SuperDARN virtual height models, *Ann. Geophys.*, *26*(4), 843–852, doi:10.5194/angeo-26-843-2008.